Supramolecular Control of Helicene CPL Emitters in Molecular Solids and Bright Nanoparticles

Stine G. Stenspil,[a] Andrew H. Olsson,[b] Rebecca Mucci,[c] Maren Pink,[b] Céline Besnard,[d] Gennaro Pescitelli,[e] Jérôme Lacour,*[c] Amar H. Flood*[b] and Bo W. Laursen,*[a]

[a] S. G. Stenspil, Prof. B. W. Laursen
Nano-Science Center & Department of Chemistry
University of Copenhagen
Universitetsparken 5, 2100 København Ø, Denmark
E-mail: bwl@chem.ku.dk

[b] A. H. Olsson, Dr. M. Pink, Prof. A. H. Flood
Department of Chemistry
Indiana University
800 East Kirkwood Ave, Bloomington, IN 47405, United States
E-mail: aflood@indiana.edu

[c] R. Mucci, Prof. J. Lacour
Department of Organic Chemistry
University of Geneva
Quai Ernest Ansermet 30, CH-1211, Geneva 4, Switzerland
E-mail: Jerome.Lacour@unige.ch

[d] Dr C. Besnard
Laboratory of crystallography
University of Geneva
Quai Ernest Ansermet 24, CH-1211, Geneva 4, Switzerland

[e] Prof G. Pescitelli
Department of Chemistry and Industrial Chemistry
University of Pisa
Via Moruzzi 13, 56124 Pisa, Italy

Supporting information for this article is given via a link at the end of the document.

Abstract: Circularly polarized luminescence (CPL) from chrial molecules is attracting much attention due to its potential in optical materials. However, formulation of CPL emitters as molecular solids typically deteriorates photophysical properties in the aggregated state leading to quenching and unpredictable changes in CPL behavior impeding materials development. To circumvent these shortcomings, a supramolecular approach can be used to isolate cationic dyes in a lattice of cyanostar-anion complexes that suppress aggregation-caused quenching and which we hypothesize can preserve the synthetically-crafted chiroptical properties. Herein, we verify that supramolecular assembly of small-molecule, ionic isolation lattices (SMILES), allows translation of molecular ECD and CPL properties to

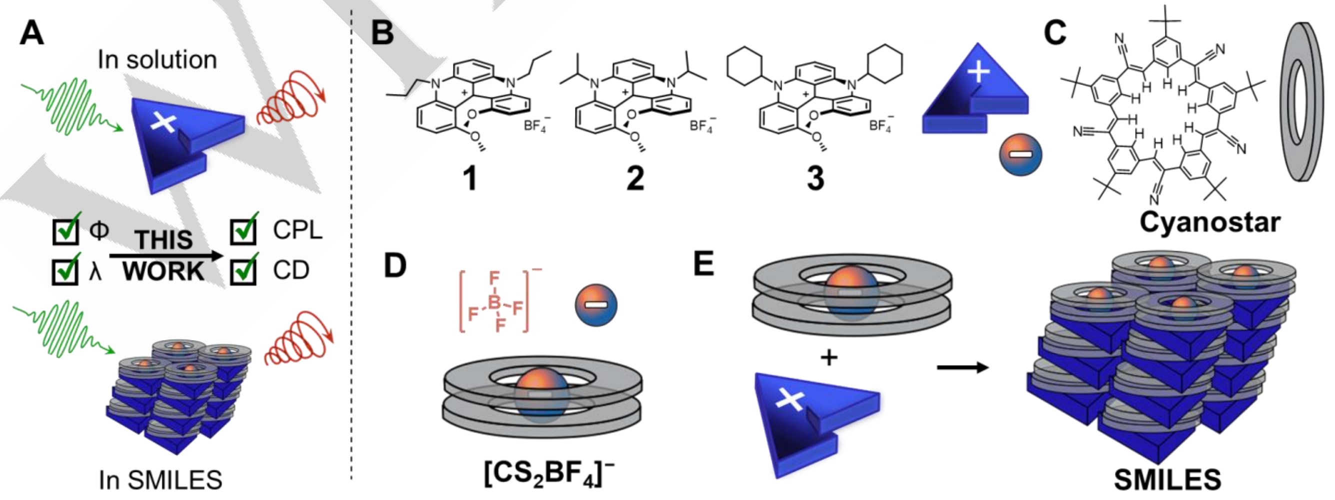

Figure 1. A) Reliable translation of chiral (ECD and CPL) and linear optical properties such as quantum yields (Φ) and spectra (λ) from molecules in solution to small-molecule, ionic isolation lattices (SMILES) materials. B) Dimethoxy-quinacridinium (DMQA) cationic [4]helicenes **1**, **2**, and **3**; (*M*)-configuration selected arbitrarily and shown as blue cartoon representation. C) Cyanostar (**CS**). D) Cyanostar-anion complex, 2:1 ratio of **CS** to the BF_4^- anion. E) Charge-by-charge assembly in SMILES.

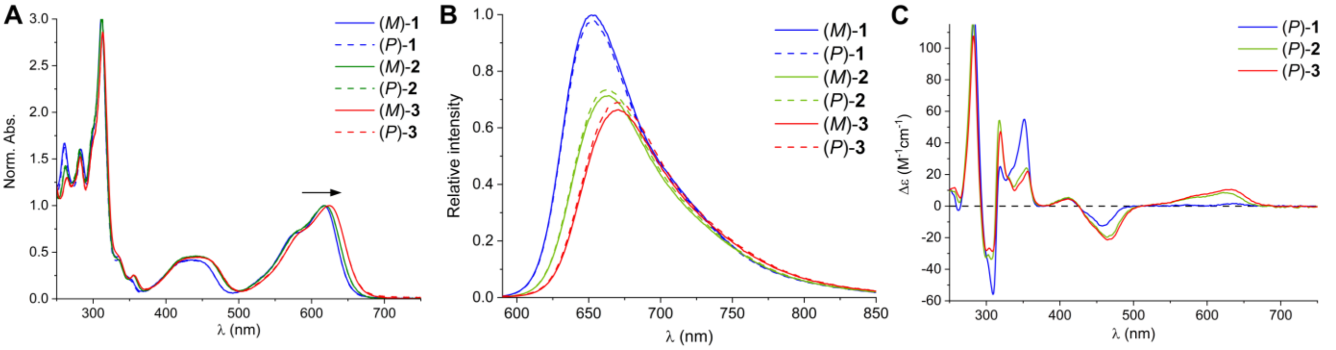

Figure 2. Spectral properties of (*M*) and (*P*) isomers of **1**-**3** in dichloromethane (DCM): (A) Normalized absorption, (B) Emission intensity of relative to **1**, excited at 560 nm, and (C) ECD spectra of (*P*)-DMQA **1**-**3** in DCM, spectra of (*M*) isomers are found in Figure S2.

solids. A series of cationic helicenes that display increasing chiroptical response, is investigated. Crystal structures of three different packing motifs all show spatial isolation of dyes by the anion complexes. We observe the photophysical and chiroptical properties of all helicenes are seamlessly translated to water soluble nanoparticles by the SMILES method. Also, a DMQA helicene is used as FRET acceptor in SMILES nanoparticles of intensely absorbing rhodamine antennae to generate an 18-fold boost in CPL brightness. These features offer promise for reliably accessing bright materials with programmable CPL properties.

Introduction

Circularly polarized luminescence (CPL) is an area under much interest and continuous development owing to its promise for use in optoelectronic devices and bioimaging.[2] These activities have resulted in development of a broad range of impressive molecular dyes based on helicenes and other chiral conjugated scaffolds.[3] In many cases, the aim is to use the chiroptical properties in optoelectronic devices that require the CPL and electronic circular dichroism (ECD) signals to be manifested in molecular solids.[4] While favorable ECD and CPL signals have been achieved in several cases, it is more typical for the properties observed in the solids to be quenched and distorted in unpredictable ways when compared to the same dyes observed in solution.[5] New methods are needed to reliably transfer CPL properties to the solid state for the creation of advanced optical materials.

The discrepancy between dilute solution and solid originates from the strong electronic coupling between chromophores in the densely packed molecular materials that alters both the photophysical and chiroptical properties.[4b,6] Aggregation-caused quenching (ACQ) and associated spectral shifts are well-known drawbacks of this coupling. While CPL has sometimes been improved when dyes are formulated into solids,[5b,7] these types of effects are neither general nor predictable. First, the prediction of molecular packing in the solid state is still in a nascent stage.[8] Despite recent investigations on the packing of neutral helicenes advances,[ref to Jelfs] these studies do not address the factors that lead to ACQ. Second, the observed changes in ECD and CPL are not straightforward to rationalize even when a crystal structure is available because we currently lack a detailed understanding of the relation between supramolecular organization and chiroptical properties.[9] Strategies to address these issues, where structure-property relationships can be placed on a firm footing, are needed to help achieve advanced CPL materials. We take steps towards addressing these issues (Figure 1) by using supramolecular organization in materials called small-molecule, ionic isolation lattices (SMILES).[10]

SMILES materials offer a general approach to turn on the fluorescence of molecular solid-state materials. We have previously shown excellent translation of optical properties of achiral cationic fluorophores from solution to solid with SMILES.[10-11] These materials use the macrocycle called cyanostar[12] (**CS**, Figure 1C) to bind the dye's negative counterions (BF_4^-) in a 2:1 ratio with high stabilities (>60 kJ mol^{-1}) thereby forming a large disc-shaped anionic complex (Figure 1D). This complex, in turn, directs the assembly of an ionic lattice (Figure 1E) to help ensure spatial isolation and electronic decoupling of the cationic fluorophores and thus counteracting ACQ in SMILES materials. This method was shown to be applicable to widely used families of cationic fluorophores, such

Table 1: Photophysical properties of DMQA derivatives in DCM. Absorption coefficient, ε, found at the first electronic transition. ^{a}Quantum yield (QY) of **2** and **3** are found relative to **1** which is obtained from Kel *et al*.[1]. ^{b}Fluorescence lifetime, τ_f, detected at 700 nm. The radiative lifetime, τ_0, is calculated as τ_f/QY. The radiative rate, k_f, is calculated from $1/\tau_0$ and the non-radiative rate, $k_{nr}=1/\tau_f - k_f$.

	λ_{max} (nm)	$\lambda_{f,max}$ (nm)	ε ($M^{-1}cm^{-1}$)	QY^a	τ_f^b (ns)	τ_0 (ns)	$k_f \cdot 10^7 (s^{-1})$	$k_{nr} \cdot 10^7 (s^{-1})$	$g_{abs} \cdot 10^{-4}$	$g_{lum} \cdot 10^{-4}$	B_{CPL} ($M^{-1}cm^{-1}$)
1	618	651	15900	*0.21*	12.6	63	1.6	6.4	0.9 -2.0	1.8 -2.5	0.4
2	619	663	14700	0.15	11.4	76	1.3	7.5	5.5 -6.7	5.6 -7.3	0.7
3	625	670	15200	0.14	10.3	73	1.4	8.3	6.2 -7.8	7.1 -8.7	0.8

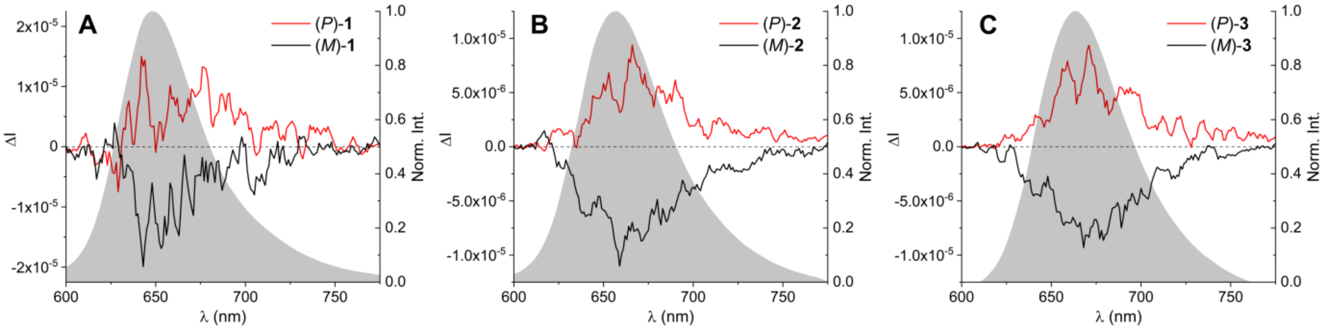

Figure 3. CPL spectra of (A) **1**, (B) **2** and (C) **3** (*P*) and (*M*) enantiomers in DCM, excited at 450 nm, total emission spectra recorded in same experiment shown in gray.

as, cyanines, rhodamines, oxazines, and trianguleniums, and found to work both in large crystals ($>\mu m$) and smaller water-soluble nanoparticles (NPs), which are promising for bioimaging applications.[10b,13] The crystal structures feature a surprisingly reliable charge-by-charge packing[8a] of cationic dyes and anion-bound complexes. Encouraged by the success of SMILES to turn on the quantum yields of emission and offer solution-like fluorescence in molecular solids and nanoparticles, SMILES materials also hold promise for seamlessly translating intrinsic chiroptical properties of helicenes into solid materials. Thus, SMILES could help accelerate development of structure-property relationships for CPL materials by disentangling molecular and supramolecular contributions to the chiroptical response of molecular helicene materials.

In this work, we conduct a proof-of-principle demonstration to verify that the ECD and CPL responses programmed into chiral dyes using covalent synthesis can be seamlessly delivered to solid materials using the SMILES method. We characterize the photophysical and chiroptical properties of a series of cationic [4]helicenes of the dimethoxy-quinacridinium (DMQA) family in the form of *n*-propyl **1**, isopropyl **2**, and cyclohexyl **3** (Figure 1B) in solution, crystals, SMILES crystals, and SMILES nanoparticles. The DMQA helicenes are attractive for this study due to their intrinsic cationic nature (a fundamental requirement for SMILES formation), their facile and flexible synthesis and resolution, and their tunable absorption and emission.[14] In this first investigation of chiral SMILES materials, near perfect translation of solution photophysical and chiroptical properties to SMILES solids was achieved (Figure 1A). The chiral dyes co-assemble with cyanostar-anion complexes into SMILES crystals to form isolation lattices. Different solvent conditions afforded the first examples of SMILES pseudo-polymorphs with three different packing motifs also including the first SMILES crystals with chiral space groups that are mirror images of each other. Each packing arrangement forms spatial isolation lattices that are responsible for the reliable transfer of linear optical properties from solution to crystal. In an effort to increase CPL brightness,[15] we used DMQA [4]helicene **3** as a chiral dopant fluorophore in non-chiral rhodamine-based SMILES nanoparticles resulting in brightness, B_{CPL}, that is amplified by a factor of 18.

Results and Discussion

Synthesis of DMQA helicenes

The synthesis of the DMQA helicenes **1**-**3** has been reported previously.[16] Gram-scale separation of the right and left-handed helicenes, of (*P*) and (*M*) configuration respectively, was achieved by chromatography (SiO_2) on neutral diastereomeric sulfoxide adducts and, after physical separation, by mild *Pummerer* fragmentation to yield the separated enantiomeric DMQAs (details in SI §2).[16]

Optical properties of DMQA helicenes in solution

Solution studies of helicenes **1**, **2,** and **3** provide a detailed mapping of photophysical and chiroptical properties in solution to be used as a frame of reference for their study as SMILES materials. Chiroptical properties of **1** have been reported in detail previously but only in part for isopropyl **2** and cyclohexyl **3**.[14d,16] From previous studies of helicene **1**, it is known that fluorescence quantum yields and lifetimes are strongly influenced by the solvent, with dichloromethane (DCM) providing most favorable emission properties.[1] Thus, we characterized the (*P*) and (*M*) enantiomers of DMQA helicenes **1**-**3** in DCM (Figure 2 and Table 1; additional data in Figures S1-S2).

Introduction of the bulkier α-branched substituents, isopropyl and cyclohexyl, on the nitrogen atoms resulted in slight red-shifts of the lowest energy absorption band from 618 nm for **1** to 625 nm for **3** (Figure S1B). A similar trend is observed in the emission spectra. Fluorescence quantum yields and lifetimes decrease modestly from **1** to **3**. Calculation of fluorescence, k_f, and non-radiative deactivation, k_{nr}, rates (Table 1) show that the decrease in quantum yields and lifetimes stem from both reductions in radiative rate and an increase in non-radiative deactivation. Most noticeably, the ECD spectra of helicenes **2** and **3** show a clear increase in dissymmetry for the lower energy $S_0 \rightarrow S_1$ absorption band (550-650 nm, Figure 2C). The dissymmetry factor is increased by a factor of ~3.7 from **1** to **3**. This increase is important on account of the fact that the first electronic transition also dictates the emission dissymmetry, and it confirms that bulky substituents on the N-atom or in adjacent positions can be used to boost intrinsic dissymmetry.[17]

The CPL spectra of (*P*) and (*M*) enantiomers of helicenes **1**-**3** were measured in DCM solution (Figures 3 and S19). They display similar increases in dissymmetry with increasing bulk of the substituents. The *n*-propyl DMQA displayed weak chiroptical emission activity for (*P*) and (*M*) enantiomers with g_{lum} = 1.8 and -2.5×10^{-4}, in line with previous reports.[14d] However, both the isopropyl and cyclohexyl derivatives **2** and **3** showed higher dissymmetry factors with 3- to 4-fold increase in their g_{lum} values to around $\pm 7 \times 10^{-4}$ (Table 1).

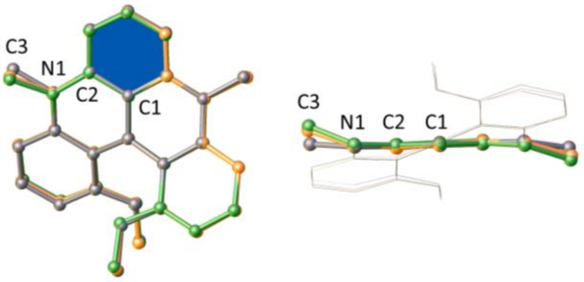

Figure 4. Superimposition of [4]helicenes **1**, **2,** and **3** represented in grey, orange and green colors, respectively. All compounds are presented with the same (*M*) configuration for convenience.

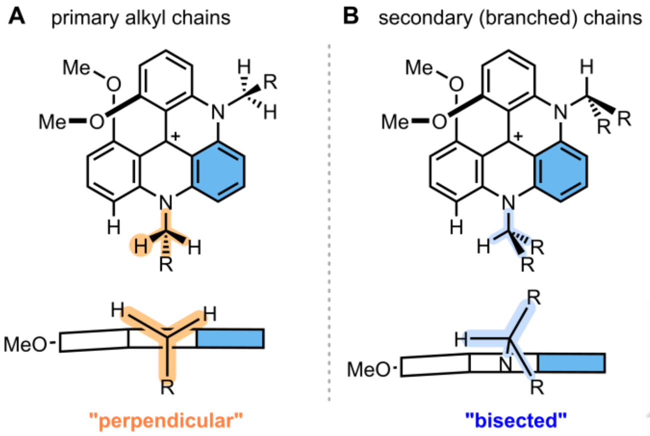

Figure 5. Nitrogen atom substitution. Side-chain orientations for primary (left) and secondary (right) alkyl groups with perpendicular and bisected conformations, respectively.

Molecular structures of DMQA [4]helicene derivatives

X-ray crystal structures of the helicenes alone were used to help pinpoint the origin of the chiroptical differences between compound **1**, carrying linear propyl chains, **2** and **3** with α-branched isopropyl and cyclohexyl substituents. For compounds (*rac*)-**1**, (*P*)-**2** and (*M*)-**3**, crystals suitable for measurements were obtained by slow diffusion of ether or toluene in DCM solutions of the dyes. The structure of compound **1** was previously reported (CCDC 205385), and the data was utilized in our analysis.[18]

Considering the rigidity of the skeleton, it is not surprising that the molecular structures present many similar bond lengths and angles (Figure 4, Table S3). These include deformations in the helicene core, which were characterized by measuring both helical dihedral angles along the internal groove and O····O distances between methoxy groups (Table S3). These geometries were also similar to previously reported derivatives.[14d] Globally, the helicene framework is very well conserved in **1**, **2** and **3** with comparable degrees of twists.

The main differences are observed for the side chains.[19] The C3 carbon atoms (Figure 4), which link alkyl residues to the helical core at N1, are either aligned (**1**) or positioned away (**2**-**3**) from the (reference blue) benzene plane (see also Table S3).[20] This observed deformation, in the case of α-branched derivatives **2** and **3**, likely results from a local strain. In fact, interactions between the helicene core and the secondary alkyl groups change the preferred conformation of the side chains from a"perpendicular" orientation with *n*-propyl **1**,[21] to "bisected" geometries for the isopropyl and cyclohexyl (Figure 5).[22] In these "bisected" conformations the hydrogen atom attached to the C3 carbons becomes almost coplanar with the ring system (see Figure S7 and S8).[22b] Overall the distortions induced by the branched side chains provoke a pyrimidalization of the nitrogen bridging atoms and those are suspected to be the origin of the enhanced chiroptical properties of **2** and **3**, compared to **1**. This was confirmed by computational studies.

TD-DFT ECD calculations run on (*P*)-**1**-**3** using input structures derived from X-ray geometries and fully re-optimized at B3LYP-D3/6-31+G(d,p) level yielded a weak $S_0 \rightarrow S_1$ band for **1** ($g_{abs} < 10^{-4}$) and a well-defined band for **2** and **3** ($g_{abs} = +6$ and $+7 \times 10^{-4}$, respectively; Figure 6A-C, solid lines). When the three substituents were truncated at the first carbon atom (C3), preserving its position and re-optimizing only the capping H atoms (Figure 6D), the three methyl-truncated structures afforded spectra almost superimposable to the full structures (Figure 6A-C, dotted lines). This result demonstrates that the deviation of C3 from the reference benzene plane, associated with a partial pyramidalization of N1, is the key structural factor determining the chiroptical response for the lowest energy transition (see SI §3 for further analysis). Furthermore, we notice that the DFT optimized structures to a very large degree reproduce the structural variations in the DMQA cores discussed above, confirming that these variations are indeed induced by the bulky side groups and not by crystal packing effects (Figure S3).

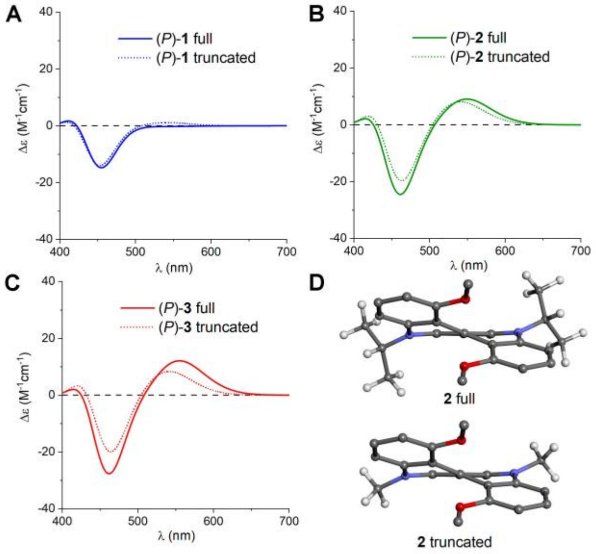

Figure 6. (A-C) TD-DFT calculated ECD spectra of [4]helicenes (*P*)-**1**-**3** (solid lines) and their analogs truncated at C3 (dotted lines). Level of calculation B3LYP/def2-TZVP/PCM(DCM)//B3LYP-D3/6-31+G(d,p)/PCM(DCM). (D) DFT-optimized structure of (*P*)-**2** (obtained starting from the X-ray geometry) and its methyl-truncated analog (obtained by truncation at C3 and re-optimization of the capping H atoms). Only H atoms belonging to the *N*-substituents are shown.

Chiral crystal structures and optical properties of SMILES materials using DMQA helicene 1 and cyanostar

Crystal structures of the enantiopure and racemic helicenes co-crystallized with cyanostar were solved to verify formation of SMILES isolation lattices. Using conditions employed previously with achiral dyes,[10a] crystals of the (*M*) isomer of helicene **1**•BF_4 salt were grown with two equivalents of cyanostar in DCM by vapor diffusion of ether (details in SI §8). The structure solution shows a chiral space group *P*1 in contrast to the centrosymmetric space group *P*-1 found for previous SMILES structures while retaining the charge-by-charge packing (Figure 7) between cationic dye and cyanostar-anion complex seen in prior SMILES crystals.[10a] Compared to prior examples, the shorter ~12 Å separation of dyes along the stack direction (Figure 7A) and the longer distance between stacks, ~20 Å (Figure 7B), lead to similar dye densities. Crystals grown using the antipodal enantiomer, (*P*)-**1**, generated an identical but mirror image structure.

While the co-crystallization of enantiopure dyes with configurationally-labile cyanostars[23] may potentially lead to chiral induction in the twisted macrocycle geometries, an enrichment in either the clockwise (*P*) or counter-clockwise (*M*) forms of the cyanostar was not observed. Instead, we saw the typical whole molecule disorder in which macrocycles on each lattice site having an admixture of both *M* and *P* enantiomers with an equal number of both present in the crystal.[12] Our crystal of the (*M*)-**1** enantiomer is exemplary. Taking the whole molecule disorder into account, the relative ratio of (*M*) and (*P*) cyanostar present is about 50:50 for each individual cyanostar. This absence of chiral induction in the cyanostar is also confirmed by the lack of ECD response in the region where cyanostar absorbs (250-350 nm) as shown for nanoparticles in Figure S16.

The absorption (black) and emission (red) spectra of (*M*)-**1** recorded in solution (Figure 8A) translate to the excitation and emission spectra of the SMILES crystal sample (Figure 8B) and nanoparticles (Figure 8C, see discussion below), which is consistent with formation of electronic isolation lattices.

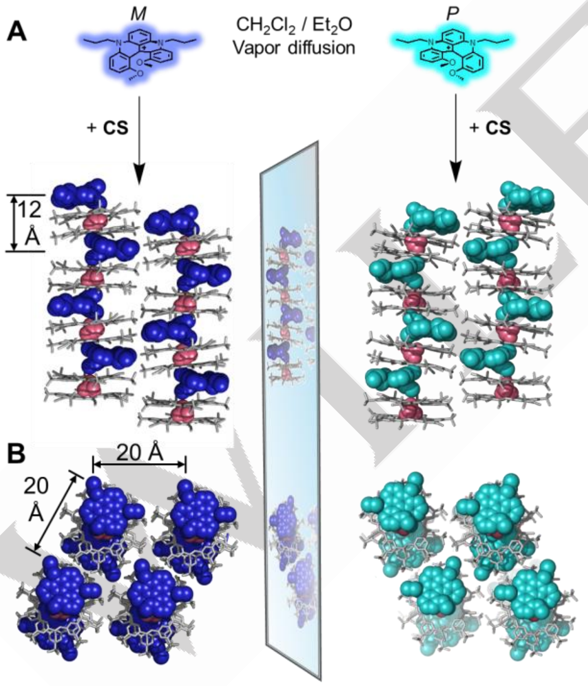

Figure 7. SMILES crystal structure of (*M*) and (*P*) isomers of **1**•(**CS**)$_2$•BF$_4$. (CCDC 2305002 and 2305003). (A) The molecular packing and dye-dye distance along the stacking direction. (B) Top down view of columnar stacks of alternating dye-anion complexes, showing lateral dye-dye distances.

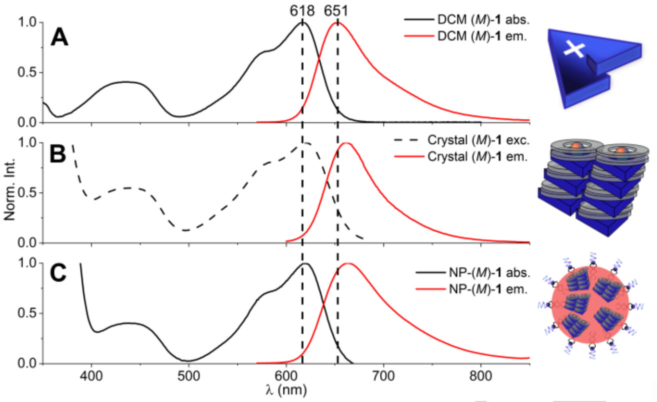

Figure 8. Normalized absorption (black), excitation (dashed) and emission (red) of (*M*)-**1** in (A) DCM solution, (B) crushed forms of single SMILES crystals (< 5 μm) of (*M*)-**1**•(**CS**)$_2$•BF$_4$ grown from DCM-ether by vapor diffusion, and (C) and SMILES nanoparticles.

New Packing in Pseudo-polymorphs of SMILES Crystals

Changes in the solvents used to grow crystals with (*P*)-**1** generated SMILES materials with the first observed variation in the packing pattern (Figure 9A). These structures have the same stoichiometry of dye and complex in the unit cell. Given that these structures have different numbers of solvents in the unit cell, they are called pseudo-polymorphs.[24]

This new SMILES pseudo-polymorph forms a spatial isolation lattice with the shortest inter-dye distance of 14 Å (Figure 9A). In these crystals, however, the dye is no longer π-stacked between two cyanostar complexes but sits at the interface of four complexes forming a pseudo-T-bone arrangement with two of them. The dye sits at an angle of ~40° to the macrocycle plane (Figure 9B). As with the first pseudo-polymorph, we do not see chiral induction from the dye onto the cyanostar.

Surprisingly, crystals composed of the racemic compound failed to grow under either of the vapor-diffusion conditions that were used with the enantiopure compounds. Use of a third condition (vapor diffusion of diethyl ether into chloroform), however, afforded crystals as a racemate with a *P*-1 space group incorporating both (*M*) and (*P*) helicenes and observation of another new pseudo-polymorph (Figure 10). There are three remarkable features of this packing arrangement. First, two dyes instead of just one are sandwiched between cyanostar-anion complexes. These dyes are arranged side-by-side but still display a large 16 Å centroid-to-centroid distance. Second, there is an intervening stack of cyanostar-anion complexes to maintain charge neutrality. The charge-alternating and charge-segregated stacks[8a] arrange into a thick-thin herringbone pattern. Third, while we observe an 83:17 *M*:*P* ratio of cyanostars on one site in the thicker charge-alternating block, in the adjacent stack of cyanostar complexes we observe *meso* diastereomers (*MP*) with 100% site occupation. The absence of whole molecule disorder in this stack is unique across all cyanostar crystal structures reported. Interestingly, the enantiopure forms of the dyes did not produce crystals under the conditions used to grow the racemate suggesting that the crystal growth conditions are mutually exclusive.

The emergence of three different SMILES packing patterns allows us to probe their impact on the optical properties. Consistent with the appearance of dye-dye isolation, excitation and emission spectra obtained from finely ground crystals show similar profiles to each other and solution spectra (Figure S11). This finding underscores the reliability of cyanostar-anion complexes in enforcing isolation lattices across multiple packing arrangements. In cases when the exact packing is either not known or not readily controlled, in thin films and nanoparticles formed under kinetic control, this observation indicates the advantage offered by cyanostar in reliably delivering an isolation lattice.

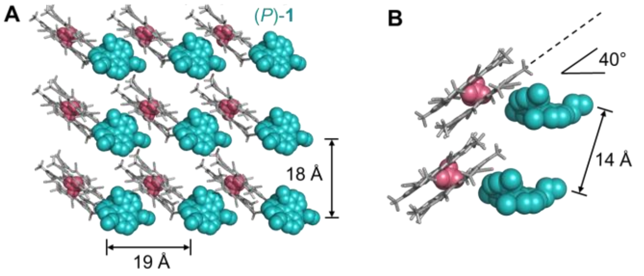

Figure 9. (A) Crystal structure of the SMILES crystal showing a pseudo-polymorph of (*P*)-**1**•(**CS**)$_2$•BF$_4$ (CCDC 2305005) and (B) the pseudo-T-bone packing. Crystals grown by hexane vapor diffusion into a chloroform solution of (*P*)-**1**•BF4^{-} with 2 equivalents of cyanostar.

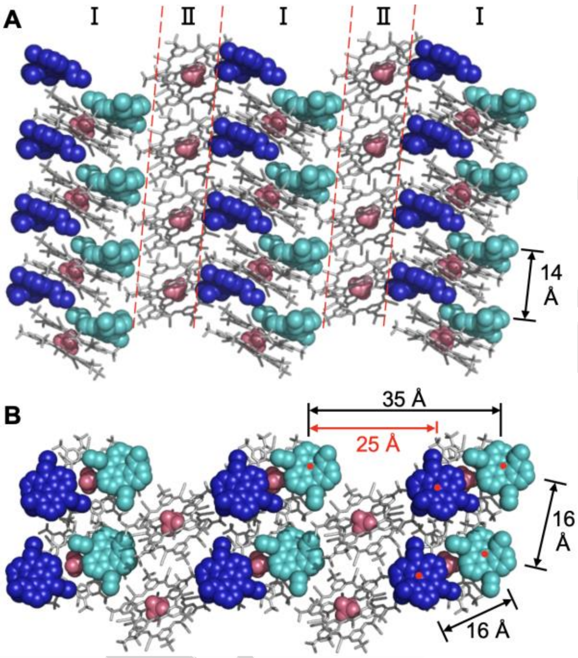

Figure 10. (A) Side view of the crystal structure of SMILES crystals with a thick-thin, I-II, herringbone packing pattern of (*rac*)-**1**•(**CS**)$_2$•BF$_4$ (CCDC 2305004). (B) top view.

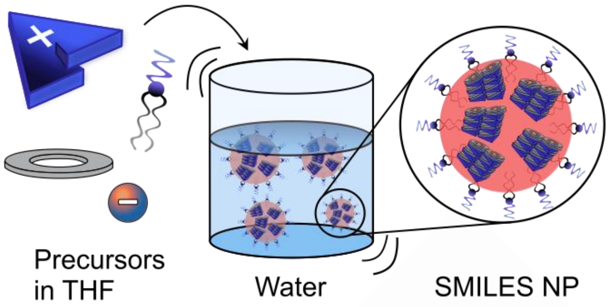

Figure 11. Preparation of fluorescent SMILES nanoparticles by nanoprecipitation of THF precursor solution in large excess of water.

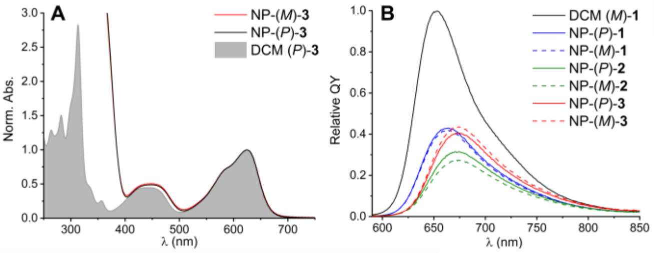

Figure 12. DMQA nanoparticles: (A) normalized absorption of NP-**3** enantiomers and (*P*)-**3** in DCM solution. (B) Relative emission of DMQA SMILES nanoparticles compared to (*M*)-**1** in DCM, excitation at 560 nm.

Chiral SMILES nanoparticles

Previously, we have shown that the SMILES approach to generating optical materials can be readily used for the producing water-soluble nanoparticles on order 20 nm in size with several different cationic dyes.[10b,11b,13] We hypothesize that the use of SMILES nanoparticles holds the potential to facilitate incorporation of CPL emitters in aqueous and biological media while also simplifying measurements of optical properties of the SMILES materials that benefit from both the isotropic and non-scattering nature of nanoparticle suspensions.

SMILES nanoparticles (NP), capped with an amphiphilic ligand (bearing on glycol and two alkyl chains) to ensure stability of the nanoparticles, were prepared using the previously developed nanoprecipitation procedure (Figure 11, details in SI §3)).[10b]

SMILES nanoparticles were formed in aqueous solution from each of the enantiomers (*M*) and (*P*) of the three DMQA fluorophores. Characterization by dynamic light scattering (DLS) failed due to the high absorption from DMQA at 633 nm interfering with the laser of the DLS instrument. For NP-(*rac*)-**1** and NP-(*P*)-**3** we found the nanoparticle size by cryo transmission electron microscopy to be ~13 nm (Figure S24).

The absorption spectra of DMQA-based SMILES nanoparticles in water show remarkably good reproduction of the solution-state spectra of the free dyes in DCM, as shown for NP-**3** (Figure 12A; spectra of NP-**1** and NP-**2** are shown in Figures S12A and B). Below 400 nm, nanoparticle absorption spectra are dominated by the intense cyanostar absorption band (Figure S12D), while the longer wavelengths show features originating exclusively from the helicenes. The emission spectra of the DMQA SMILES nanoparticles are slightly red-shifted and less intense compared to the dyes alone in dilute DCM solutions of the same optical density and concentration (Figure 12B). Thus, nanoparticles have quantum yields of 5-8% compared to 14-20% for the helicenes in dilute DCM solution (Tables 1 and 2). The spectral width and position of the nanoparticle's emission spectra, however, match very well with those measured in acetonitrile (MeCN) solutions (Figure S13), indicating that the dielectric environment in the SMILES nanoparticles is more comparable to MeCN than the less polar DCM. Quantum yields in MeCN (8%) are also comparable to nanoparticles.[1] Similarly, fluorescence lifetimes of the nanoparticles are 5-6 ns, compared to 5.5 ns in MeCN and 12 ns in DCM. The similarity of quantum yield and lifetime to MeCN solutions may however be a coincidence. The nanoparticles display multi-exponential fluorescence decays with components as long as ~9 ns (Table S13 and Figure S14) indicating that the quantum yields and fluorescence lifetimes are limited by energy migration to trap states and not by a general, faster internal conversion for DMQA dyes in the SMILES lattice.[11a] To emphasize that SMILES are vital in the retention of the optical properties, we prepared non-SMILES nanoparticles without cyanostar for both racemic **3** and (*P*)-**3** (see SI §3 for details).

Table 2: Optical properties of DMQA nanoparticles. ^{a}Relative QY measured relative to **1** in DCM[1] and corrected for refractive index. ^{b}Intensity average lifetime measured on nanoparticles consisting of the (*P*) enantiomer detected at 700 nm.

	RQY^a	$\tau_{av}{}^b$ (ns)	$g_{abs} \cdot 10^{-4}$	$g_{lum} \cdot 10^{-4}$	$B_{CPL,em}$ ($M^{-1}cm^{-1}$)
NP-**1**	0.08	6.3	1.8 -1.4	2.2 -2.0	0.1
NP-**2**	0.05	5.0	6.5 -7.1	5.7 -6.8	0.2
NP-**3**	0.08	6.4	7.0 -8.3	7.4 -8.0	0.4

The resulting non-SMILES materials show a broadened absorption band (Figure S15A). Emission from these particles also show signs of aggregation with significant quenching of the emission yield, decreases in fluorescence lifetime, and red-shifted spectra (Figures S15C and D and Table S15). Furthermore, the non-SMILES particles display a new blue shifted emission at ~600 nm not observed in the SMILES formulations. All these features are the result of aggregation and allow us to conclude that the formation of SMILES lattices is essential for preventing ACQ.

The ECD spectra of SMILES nanoparticles (Figures 13 and S16) show extraordinarily good reproduction of the solution state chiroptical properties with g_{abs} values on par with solution measurements (Table 2). Contrary to the absorption spectra, the features in the ECD spectra of the DMQA dyes in the UV region are not hidden under the cyanostar absorption. All ECD signals down to 250 nm are identical to those observed for solutions of the dyes alone ruling out chiral induction in the $[\mathbf{CS_2}{\bullet}BF_4]^-$ anion complexes and any supramolecular couplings in the nanoparticle SMILES lattice, also as seen from the SMILES crystal structures above.

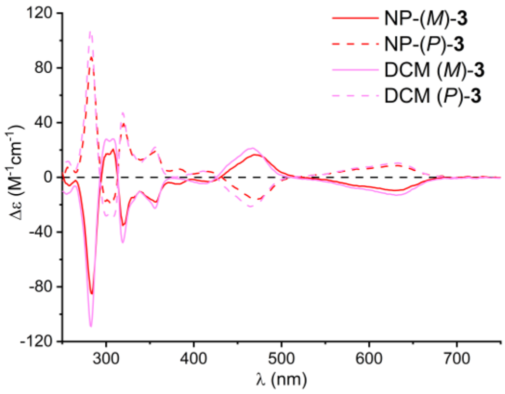

Figure 13. ECD spectra of **3** (*P*) and (*M*) enantiomers in DCM solution and SMILES nanoparticles.

CPL spectra of the SMILES nanoparticles consisting of the DMQA helicenes **1-3** (Figure S20) were comparable to the solution CPL of the dyes alone (Figure 3). Beyond the weaker signal, which stems from the lower quantum yield, we found the same g_{lum} values as in solution (compare Tables 2 and 1). Even though the fluorescence intensity is decreased, it is extraordinary that the SMILES nanoparticles exhibit this precise reproduction of solution state chiroptical properties when formulated into a dense molecular material.

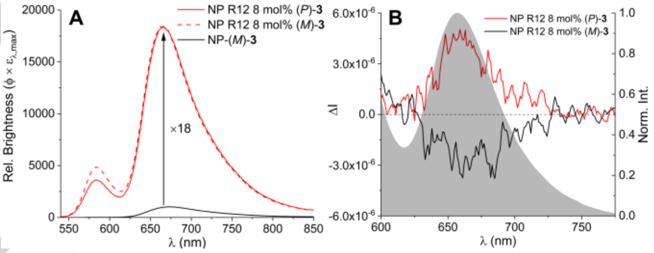

Figure 14. (A) Relative brightness of nanoparticle **R12** with 8 mol% **3** compared to NP-**3**. (B) CPL of nanoparticle **R12** with 8 mol% **3** (*P*) and (*M*) enantiomers excitation at 535 nm.

Enhancement of CPL brightness

For applications of CPL dyes, the corresponding brightness (B_{CPL}) is often used as a figure of merit. It compiles the emission brightness with the asymmetry factor (Equation 1).[15]

$$\text{(Eq. 1)} \qquad B_{\mathrm{CPL}} = \varepsilon \cdot \Phi \cdot \frac{|g_{lum}|}{2}$$

To increase the CPL brightness of the SMILES nanoparticles, we introduce the DMQA derivatives as a dopant in a rhodamine-based SMILES matrix using the lipophilic rhodamine, **R12**.[10b,25] As a result of the good spectral overlap between **R12** emission and DMQA absorption (Figure S17), this donor-acceptor pair is expected to be an efficient system for FRET.[11a,13] This system has several advantages: 1) Due to efficient energy migration and transfer, only a small amount of the precious enantiopure DMQA is needed. 2) By choosing specific FRET pairs, absorption and emission wavelengths can be tuned independently to suit specific applications. 3) In this case, the very large absorption coefficient of **R12** ($\varepsilon \approx$ 100 000 M^{-1} cm^{-1}), seven times that of DMQA, will help boost B_{CPL}. A high CPL brightness will increase the applicability of these systems in various applications, e.g., bioimaging where a high signal-to-noise ratio is critical. The use of a FRET system also generates a large Stokes shift without compromising on the selection of an optimal absorption wavelength for conducting CPL measurements where instrument slits are often very wide.

FRET nanoparticles composed of **R12** SMILES and doped with 1-10 mol% of (*rac*)-**1** were prepared and characterized to find the optimal dopant-to-antenna ratio. The size of the doped nanoparticles was found by DLS to be 17 Å, irrespectively of the doping degree (SI §14). In this case, the lower optical density at 633 nm (at low doping levels) did not interfere with the measurement. The absorption spectra (Figure S18A) are dominated by the cyanostar absorption below 400 nm and the **R12** absorption at ~560 nm while the DMQA absorption (~625 nm) is hardly discernable from the baseline. The emission spectra (Figure S18B), however, show a larger difference between the different doping ratios. The nanoparticles with low doping percentages of 1-4 mol% do not achieve efficient energy transfer, and there is still a large residual emission from the **R12** antenna. Nanoparticles doped with 6-10 mol% of **1** show better energy transfer with residual **R12** emission constituting approximately 10% of the total emission. In this doping regime, residual **R12** emission is only decreased slightly with further doping and relative fluorescence intensities are practically unchanged (Figure S18C). For a compromise between maximal absorption efficiency and energy transfer, we chose to use 8 mol% doping for further studies. Fluorescence lifetimes of the various doping levels also displayed little variation (Table S16). However, we noticed that the fluorescence lifetime of the DMQA emission of all doped nanoparticles is increased to 10 ns compared to neat DMQA nanoparticles (with τ = 6.3 ns). We interpret this improvement as a result of less efficient energy migration between DMQA units and to dark traps now that the DMQA dyes are more separated.[11a,13]

The emission spectra (Figure 14A) of **R12** SMILES nanoparticles doped with 8 mol% (*P*)-**3** or (*M*)-**3** also show fluorescence lifetimes measured from the DMQA band at 700 nm increasing to 10 ns (Table 3). The improved emission properties are further confirmed by the fluorescence quantum yield increasing to 19% when calculated for the DMQA emission band alone and compared to 8% for the SMILES nanoparticles composed only of **3**. The increased quantum yield and lifetime highlight the additional advantage of doping by outcompeting energy transfer to trap states. Overall, the antenna effect of **R12** and the improved quantum yield results in an improvement of brightness by a factor of 18 compared to the neat **3** SMILES nanoparticles.

The CPL signal (Figure 14B) shows that excitation of the non-chiral rhodamine antenna still produces chiral luminescence after energy transfer to the chiral dopant. The g_{lum} values of the doped nanoparticles are as expected similar to **3** both in DCM solution and as neat nanoparticles (Table 3), confirming that the isolated DMQA dyes act as the emitters in the doped nanoparticles.

The DMQA helicenes in DCM solution display moderate CPL brightnesses (B_{CPL} = 0.4 to 0.8 M^{-1} cm^{-1}, Table 1) that are comparable to other reported helicenes.[15] In the neat nanoparticles, the quantum yield is reduced, which lowers the brightness per emitter ($B_{CPL,em.}$ = 0.1 to 0.4 M^{-1} cm^{-1}, Table 2). However, DMQA dyes have very low quantum yields when dissolved in water.[1,26] These problems are mitigated when the DMQAs are protected from water inside the SMILES nanoparticles.

Table 3: Optical properties of **R12** SMILES nanoparticles doped with 8 mol% of (*M*) or (*P*)-**3**. [a]Intensity average fluorescence lifetime detected at 700 nm. [b]QY measured relative to cresyl violet in methanol integrated from 613 nm.

	λ_{max} (nm)	$\lambda_{f,max}$ (nm)	τ_{av}[a] (ns)	QY[b]	$g_{lum}\cdot10^{-4}$	$B_{CPL,em.}$ (M^{-1}cm^{-1})
R12 (*P*) -**3**	562	666	10.8	0.19	8.3	6.4
R12 (*M*) -**3**	562	662	10.2	-	-5.6	

Concerning the brightness of nanoparticles, special consideration is needed as the nanoparticles consist of multiple fluorophores. For imaging applications, where a dye or a nanoparticle acts as a label (e.g., on a protein), it makes sense to report the brightness of the label, which then becomes much larger for the nanoparticles. In the case of **R12** nanoparticles containing **3** doped into the SMILES lattice, the brightness improved by a factor of 18 (due to the high absorption coefficient of rhodamine and the elevated quantum yield of DMQA when present as a diluted dopant). As the g_{lum} is unchanged, this operation results in a similar enhancement of $B_{CPL,em.}$ to 6.4 M^{-1} cm^{-1} (Table 3). The entire nanoparticle, with a diameter of 17 nm, contains approximately 300 dyes[10b,11b] yielding a CPL brightness of $B_{CPL,NP}$ = 2000 M^{-1} cm^{-1} for the nanoparticle as a single label.

Conclusions

We seamlessly translated the optical and chiroptical properties of DMQA-based helicenes to molecular solids for the first time by using the SMILES approach. By appending branched sterically-demanding substituents onto the cationic [4]helicene DMQA, from *n*-propyl to isopropyl and cyclohexyl, both absorption and emission dissymmetry factors were enhanced, as a consequence of slight structural diversity around the nitrogen atoms. The (*M*) and (*P*) isomers, and the racemic mixture of the *n*-propyl helicene **1** crystallize in SMILES as spatial isolation lattices. Three different forms of isolation lattices were observed featuring similarly large, ≥12 Å, inter-dye distances. The translation of absorption and emission spectra from dilute solutions to crystalline materials demonstrate that strong electronic interactions between DMQA chromophores are minimized in the SMILES materials. Isolation lattices are formed in all three unique packing patterns formed between DMQA and cyanostar macrocycles. High dissymmetry was observed in SMILES nanoparticles of helicenes **2** and **3** with three-fold improvements in quantum yields compared to aggregates of DMQA dyes in water. To further increase CPL brightness, we introduced DMQA **3** as a dopant into a highly absorbing rhodamine SMILES nanoparticles where efficient energy migration and retention of chiral emission generated an 18-fold enhancement in CPL brightness of B_{CPL} = 6.4 M^{-1} cm^{-1} per dye, and a CPL brightness per nanoparticle of $B_{CPL,NP}$ = 2000 M^{-1} cm^{-1}. The ability of the SMILES strategy to deliver intrinsic molecular chiroptical properties to molecular solids may help to bridge the gap between molecular design and optical materials applications.

Supporting Information

Experimental details concerning preparation of samples, micrographs, crystallographic tables and additional spectra can be found in the supporting information.

Author contributions

SGS carried out solution and nanoparticle characterization. AHO conducted SMILES crystal growth and spectroscopy. RM synthesized and carried out chiral separation of the compounds. MP and CB carried out crystallography of the SMILES and DMQA crystals respectively. GP run DFT calculations and analyzed the results. BWL, AHF and JL assisted discussions and supervised the project.

Acknowledgements

This work was supported by the Independent Research Fund Denmark (DFF-0136-00122B). A.H.F. acknowledges support from the US National Science Foundation (DMR-2118423). We also thank the University of Geneva and the Swiss National Science Foundation for financial support (Grants 200020-184843, 200020-207539). CCDC 2319500 and 2319499 were obtained by Antoine Wallabregue, Dr Kévin Martin and Dr Laure Guénée. Support for the acquisition of the Bruker Venture D8 diffractometer through the Major Scientific Research Equipment Fund from the President of Indiana University and the Office of the Vice President for Research at Indiana University is gratefully acknowledged. G.P. gratefully acknowledges the University of Pisa for the availability of high-performance computing resources and support through the service computing@unipi.

Keywords: CPL • fluorescent nanoparticles • helicene • SMILES • solid-state fluorescence

References

[1] O. Kel, P. Sherin, N. Mehanna, B. Laleu, J. Lacour, E. Vauthey, *Photochem. Photobiol. Sci.* **2012**, *11*, 623-631.

[2] a) P. Stachelek, L. MacKenzie, D. Parker, R. Pal, *Nat. Commun.* **2022**, *13*, 553; b) T. Mori, *Circularly Polarized Luminescence of Isolated Small Organic Molecules*, 1 ed., Springer Singapore, **2020**; c) F. Furlan, J. M. Moreno-Naranjo, N. Gasparini, S. Feldmann, J. Wade, M. J. Fuchter, *Nat. Photonics* **2024**.

[3] a) H. Kubo, T. Hirose, T. Nakashima, T. Kawai, J.-y. Hasegawa, K. Matsuda, *J. Phys. Chem. Lett.* **2021**, *12*, 686-695; b) T. Mori, *Chem. Rev.* **2021**, *121*, 2373-2412; c) S. T. Bao, H. Jiang, C. Schaack, S. Louie, M. L. Steigerwald, C. Nuckolls, Z. Jin, *J. Am. Chem. Soc.* **2022**, *144*, 18772-18777; d) S. K. Pedersen, K. Eriksen, M. Pittelkow, *Angew. Chem. Int. Ed.* **2019**, *58*, 18419-18423; e) C. Maeda, K. Nagahata, T. Shirakawa, T. Ema, *Angew. Chem. Int. Ed.* **2020**, *59*, 7813-7817; f) X. Tian, K. Shoyama, B. Mahlmeister, F. Brust, M. Stolte, F. Würthner, *J. Am. Chem. Soc.* **2023**; g) W. Niu, Y. Fu, Q. Deng, Z.-L. Qiu, F. Liu, A. A. Popov, H. Komber, J. Ma, X. Feng, *Angew. Chem. Int. Ed.* **2024**, *63*, e202319874; h) I. Shioukhi, H. Batchu, G. Schwartz, L. Minion, Y. Deree, B. Bogoslavsky, L. J. W. Shimon, J. Wade, R. Hoffman, M. J. Fuchter, G. Markovich, O. Gidron, *Angew. Chem. Int. Ed.* **2024**, *63*, e202319318.

[4] a) L. Wan, Y. Liu, M. J. Fuchter, B. Yan, *Nat. Photonics* **2023**, *17*, 193-199; b) E. Peeters, M. P. T. Christiaans, R. A. J. Janssen, H. F. M. Schoo, H. P. J. M. Dekkers, E. W. Meijer, *J. Am. Chem. Soc.* **1997**, *119*, 9909-9910; c) K. Dhbaibi, L. Abella, S. Meunier-Della-Gatta, T. Roisnel, N. Vanthuyne, B. Jamoussi, G. Pieters, B. Racine, E. Quesnel, J. Autschbach, J. Crassous, L. Favereau, *Chem. Sci.* **2021**, *12*, 5522-5533; d) C. Gedeon, N. Del Rio, F. Furlan, A. Taddeucci, N. Vanthuyne, V. G. Gregoriou, M. J. Fuchter, G. Siligardi, N. Gasparini, J. Crassous, C. L. Chochos, *Adv. Mater.* **2024**, *36*, 2314337.

[5] a) K.-F. Zhang, N. Saleh, M. Swierczewski, A. Rosspeintner, F. Zinna, G. Pescitelli, C. Besnard, L. Guénée, T. Bürgi, J. Lacour, *Angew. Chem. Int. Ed.* **2023**, *62*, e202304075; b) J. Wade, J. R. Brandt, D. Reger, F. Zinna, K. Y. Amsharov, N. Jux, D. L. Andrews, M. J. Fuchter, *Angew. Chem. Int. Ed.* **2021**, *60*, 222-227.

[6] J. Gierschner, J. Shi, B. Milián-Medina, D. Roca-Sanjuán, S. Varghese, S. Park, *Adv. Opt. Mater.* **2021**, *9*, 2002251.

[7] a) F. Song, Z. Xu, Q. Zhang, Z. Zhao, H. Zhang, W. Zhao, Z. Qiu, C. Qi, H. Zhang, H. H. Y. Sung, I. D. Williams, J. W. Y. Lam, Z. Zhao, A. Qin, D. Ma, B. Z. Tang, *Adv. Funct. Mater.* **2018**, *28*, 1800051; b) J. M. Moreno-Naranjo, F. Furlan, J. Wang, S. T. J. Ryan, T. Matulaitis, Z. Xu, Q. Zhang, L. Minion, M. Di Girolamo, T. Jávorfi, G. Siligardi, J. Wade, N. Gasparini, E. Zysman-Colman, M. J. Fuchter, *Adv. Mater.*, *n/a*, 2402194.

[8] a) Y. Haketa, S. Sasaki, N. Ohta, H. Masunaga, H. Ogawa, N. Mizuno, F. Araoka, H. Takezoe, H. Maeda, *Angew. Chem. Int. Ed.* **2010**, *49*, 10079-10083; b) G. R. Desiraju, *J. Am. Chem. Soc.* **2013**, *135*, 9952-9967.

[9] G. Albano, G. Pescitelli, L. Di Bari, *Chem. Rev.* **2020**, *120*, 10145-10243.

[10] a) C. R. Benson, L. Kacenauskaite, K. L. VanDenburgh, W. Zhao, B. Qiao, T. Sadhukhan, M. Pink, J. Chen, S. Borgi, C.-H. Chen, B. J. Davis, Y. C. Simon, K. Raghavachari, B. W. Laursen, A. H. Flood, *Chem* **2020**, *6*, 1978-1997; b) J. Chen, S. M. A. Fateminia, L. Kacenauskaite, N. Bærentsen, S. G. Stenspil, J. Bredehoeft, K. L. Martinez, A. H. Flood, B. W. Laursen, *Angew. Chem. Int. Ed.* **2021**, *60*, 9450–9458.

[11] a) L. Kacenauskaite, S. G. Stenspil, A. H. Olsson, A. H. Flood, B. W. Laursen, *J. Am. Chem. Soc.* **2022**, *144*, 19981-19989; b) J. Chen, S. G. Stenspil, S. Kaziannis, L. Kacenauskaite, N. Lenngren, M. Kloz, A. H. Flood, B. W. Laursen, *ACS Applied Nano Materials* **2022**, *5*, 13887-13893.

[12] S. Lee, C.-H. Chen, A. H. Flood, *Nat. Chem.* **2013**, *5*, 704-710.

[13] S. G. Stenspil, J. Chen, M. B. Liisberg, A. H. Flood, B. W. Laursen, *Chem. Sci.* **2024**.

[14] a) B. W. Laursen, F. C. Krebs, *Angew. Chem. Int. Ed.* **2000**, *39*, 3432-3434; b) C. Herse, D. Bas, F. C. Krebs, T. Bürgi, J. Weber, T. Wesolowski, B. W. Laursen, J. Lacour, *Angew. Chem. Int. Ed.* **2003**, *42*, 3162-3166; c) J. Bosson, N. Bisballe, B. W. Laursen, J. Lacour, in *Helicenes*, **2022**, pp. 127-165; d) I. H. Delgado, S. Pascal, A. Wallabregue, R. Duwald, C. Besnard, L. Guénée, C. Nançoz, E. Vauthey, R. C. Tovar, J. L. Lunkley, G. Muller, J. Lacour, *Chem. Sci.* **2016**, *7*, 4685-4693; e) M. M. Hossain, A. C. Shaikh, R. Kaur, T. L. Gianetti, *J. Am. Chem. Soc.* **2024**, *146*, 7922-7930; f) B. Fabri, T. Funaioli, L. Frédéric, C. Elsner, E. Bordignon, F. Zinna, L. Di Bari, G. Pescitelli, J. Lacour, *J. Am. Chem. Soc.* **2024**, *146*, 8308-8319.

[15] L. Arrico, L. Di Bari, F. Zinna, *Chem. Eur. J.* **2021**, *27*, 2920-2934.

[16] B. Laleu, P. Mobian, C. Herse, B. W. Laursen, G. Hopfgartner, G. Bernardinelli, J. Lacour, *Angew. Chem. Int. Ed.* **2005**, *44*, 1879-1883.

[17] a) H. Tanaka, Y. Inoue, T. Mori, *ChemPhotoChem* **2018**, *2*, 386-402; b) Y. Nikolova, B. Fabri, P. Moneva Lorente, A. Guarnieri-Ibáñez, A. de Aguirre, Y. Soda, G. Pescitelli, F. Zinna, C. Besnard, L. Guénée, D. Moreau, L. Di Bari, E. Bakker, A. I. Poblador-Bahamonde, J. Lacour, *Angew. Chem. Int. Ed.* **2022**, *61*, e202210798; c) M. Cei, L. Di Bari, F. Zinna, *Chirality* **2023**, *35*, 192-210.

[18] Deposition numbers 205385, 2319500, 2319499 (for (*rac*)-**1**), 2319498 (for (*P*)-**2**), 2319497 (for (*M*)-**3**), 2305002 and 2305003 (for SMILES (*M*)-**1** and (*P*)-**1**), 2305005 (for SMILES (*P*)-**1** T-bone) and 2305004 (for SMILES (*rac*)-**1** dimer) contain the supplementary crystallographic data for this paper. These data are provided free of charge by the joint Cambridge Crystallographic Data Centre.

[19] Structures of (*P*)-**2** and (*M*)-**3** both contain three crystallographically independent molecules per asymmetric unit (Figure S8).

[20] We observe torsion angles C1-C2-N1-C3 averaging 158(4)° for 2, 159(2)° for 3, 168(3)° for **1**, and 168(5)° for **1** included in the SMILES crystals (see below). Also, the distance of the C3 atoms to the plane defined by the central benzene ring averages 0.55(2) Å for **2** and 0.59(8) Å for **3** versus 0.26(10) Å in **1** and 0.31(16) Å for **1** in SMILES

[21] P. Ondrisek, M. Elie, M. Pupier, A. de Aguirre, A. I. Poblador-Bahamonde, C. Besnard, J. Lacour, *Chem. Eur. J.* **2022**, *28*, e202104405.

[22] a) U. Berg, T. Liljefors, C. Roussel, J. Sandström, *Acc. Chem. Res.* **1985**, *18*, 80-86; b) B. Laleu, C. Herse, B. W. Laursen, G. Bernardinelli, J. Lacour, *J. Org. Chem.* **2003**, *68*, 6304-6308.

[23] Y. Liu, A. Singharoy, C. G. Mayne, A. Sengupta, K. Raghavachari, K. Schulten, A. H. Flood, *J. Am. Chem. Soc.* **2016**, *138*, 4843-4851.

[24] A. Nangia, *Cryst. Growth Des.* **2006**, *6*, 2-4.

[25] I. Shulov, S. Oncul, A. Reisch, Y. Arntz, M. Collot, Y. Mely, A. S. Klymchenko, *Nanoscale* **2015**, *7*, 18198-18210.

[26] O. Kel, A. Fürstenberg, N. Mehanna, C. Nicolas, B. Laleu, M. Hammarson, B. Albinsson, J. Lacour, E. Vauthey, *Chem. Eur. J.* **2013**, *19*, 7173-7180.